Photochemical and thermal isomerizations of C2h and C2v forms of para-benzoquinone dioxime: A matrix-isolation study

ARTICLE *in* JOURNAL OF MOLECULAR STRUCTURE · JULY 2010

Impact Factor: 1.6 · DOI: 10.1016/j.molstruc.2010.03.036

4 AUTHORS, INCLUDING:

Leszek Lapinski
Polish Academy of Sciences
124 PUBLICATIONS **2,603** CITATIONS
SEE PROFILE

Michal F Rode
Institute of Physics of the Polish Academy o…
31 PUBLICATIONS **420** CITATIONS
SEE PROFILE

Maciej J Nowak
Institute of Physics of the Polish Academy o…
107 PUBLICATIONS **2,804** CITATIONS
SEE PROFILE

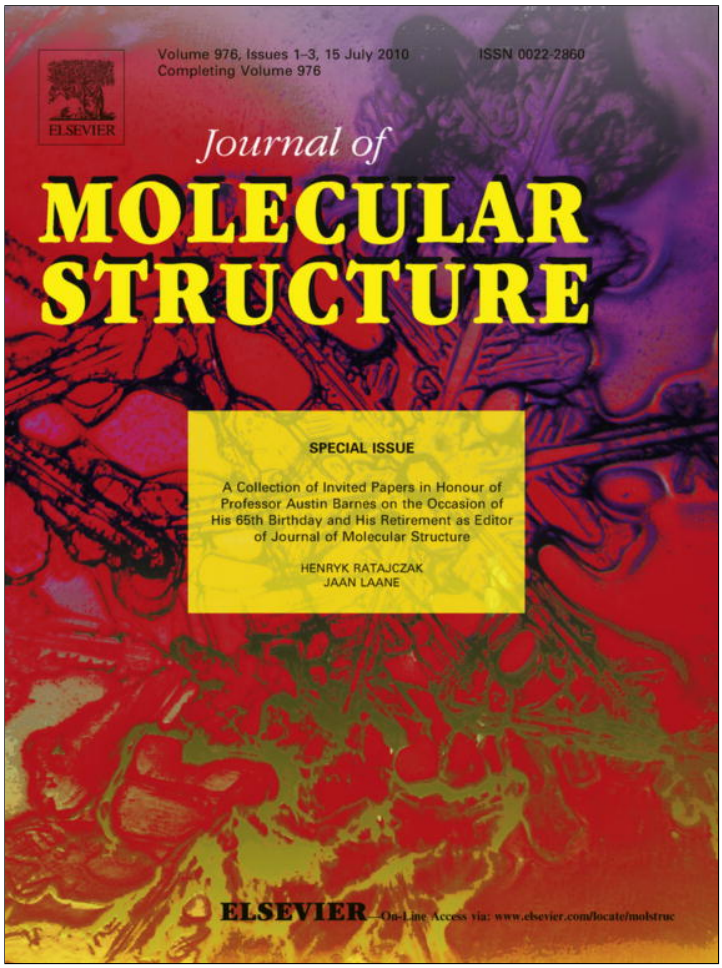

Journal of Molecular Structure 976 (2010) 181–189

Contents lists available at ScienceDirect

Journal of Molecular Structure

journal homepage: www.elsevier.com/locate/molstruc

Photochemical and thermal isomerizations of C_{2h} and C_{2v} forms of *para*-benzoquinone dioxime: A matrix-isolation study

Leszek Lapinski, Tetyana Stepanenko, Michal F. Rode, Maciej J. Nowak *

Institute of Physics, Polish Academy of Sciences, Al. Lotnikow 32/46, 02-668 Warsaw, Poland

ARTICLE INFO

Article history:
Received 13 January 2010
Received in revised form 5 March 2010
Accepted 5 March 2010
Available online 16 March 2010

Dedicated to Professor Austin J. Barnes on the occasion of his 65th birthday.

Keywords:
Para-benzoquinone dioxime
Syn
Anti
Conical intersection
Photochemistry
Matrix isolation

ABSTRACT

The C_{2h} and C_{2v} isomers of *para*-benzoquinone dioxime were studied using matrix isolation technique combined with infrared spectroscopy. The energies of these two forms were theoretically estimated (at the MP2 and CASSCF) to be nearly equal, with the C_{2h} isomer slightly more stable (by 1–2 kJ mol^{-1}). Both C_{2h} and C_{2v} forms were observed in low-temperature Ar matrices. It was experimentally found that the population ratio of the two isomers depends on the conditions of preparation of the solid *para*-benzoquinone dioxime sample used for deposition of the matrix. UV irradiation of the matrix-isolated *para*-benzoquinone dioxime led to a photochemical transformation of the C_{2v} isomer into the C_{2h} form. These findings allowed separation of the infrared spectra of the two isomers. The assignment of the C_{2v} structure to the substrate of the phototransformation as well as identification of the C_{2h} photoproduct structure was achieved by comparison of the experimental IR spectra with the spectra theoretically predicted at the DFT(B3LYP)/6-31++G(d,p) level. Complementarily to the experimental observation of the $C_{2v} \rightarrow C_{2h}$ photoisomerization, the methods of computational photochemistry were employed to calculate potential energy surfaces of the ground (S_0) and the first excited singlet (S_1) electronic states of *para*-benzoquinone. These calculations, carried out at the CASSCF level, resulted in localization of a conical intersection between the S_0 and S_1 states. At the optimized geometry of the conical intersection point, one of the hydroxylimino groups was found to adopt a perpendicular orientation with respect to the six-membered ring, whereas the other hydroxylimino group remained coplanar with the ring.

1. Introduction

Photochemistry of compounds with imine C=N bond is similar to that of systems with ethylene C=C fragment. In both cases, the first excited singlet state (S_1) has a potential energy surface with a single minimum placed at geometry similar to that corresponding to the top of the ground-state (S_0) barrier (transition state) between the *syn* and *anti* (or *cis* and *trans*) isomers. Schematic representations of the ground and excited state potential energy surfaces are presented in the classic photochemistry textbooks [1,2], as well as in papers describing particular cases of the *syn–anti* phototransformation [3,4]. After excitation to S_1 a system relaxes either back to the initial isomer or to the second structure with the substituent(s) rotated by 180°. In the latter case, the *syn–anti* (or *cis–trans*) photoisomerization occurs.

The photoinduced *syn–anti* (or *anti–syn*) isomerization reactions in oximes (benzaldoximes and related compounds) have been studied since the first years of the twentieth century [5,6]. These investigations were reviewed in Refs. [7,8]. Analogous reactions occurring in oximes that contain a C=N double bond attached directly to the ring have not been widely studied and the reported cases are quite scarce [9,10]. Recently, we found that the photoinduced *syn–anti* isomerization reaction occurs in N^4-hydroxycytosines and N^2-hydroxyisocytosine [3,4,11,12]. These compounds are obtained in reactions of hydroxylamine (known mutagen) with cytosines (or isocytosine). Depending on the *syn* or *anti* orientation of the oxime group, the promutagenic N^4-hydroxycytosines can base-pair either with adenine or with guanine.

Para-benzoquinone dioxime (PBQDO), studied in the present work, also belongs to the category of oximes with a C=N group directly attached to a six-membered ring. This compound can exist in two isomeric forms differing by 180° torsion of one OH group around the C=N bond. The high symmetry of both C_{2h} and C_{2v} isomers (Scheme 1) makes PBQDO an attractive case to study.

2. Experimental

Para-benzoquinone dioxime used in this study was a commercial product supplied by Aldrich. Prior to the matrix-isolation experiments, solid PBQDO was sublimated (at 383 K or at 433 K) in a glass tube sealed under vacuum. In order to prepare an Ar

* Corresponding author. Fax: +48 22 843 0926.
E-mail address: mjnow@ifpan.edu.pl (M.J. Nowak).

0022-2860/$ - see front matter © 2010 Elsevier B.V. All rights reserved.
doi:10.1016/j.molstruc.2010.03.036

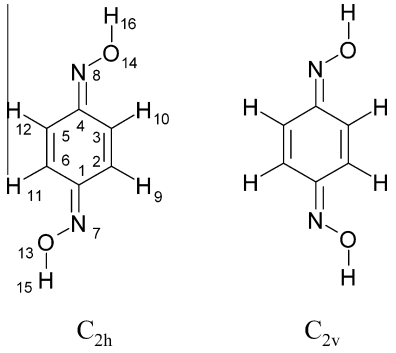

Scheme 1. Structures and atom numbering of C_{2h} and C_{2v} isomers of PBQDO.

matrix containing isolated PBQDO monomers, solid sample of the compound was heated (to 360 K) in a miniature glass oven placed in the vacuum chamber of a continuous-flow helium cryostat. The vapors of PBQDO were deposited, together with a large excess of argon, on a CsI window cooled to 10 K. Argon of spectral purity (6.0), supplied by Linde AG was used in the present experiments as a matrix gas. The infrared spectra were recorded with 1 cm^{-1} resolution using a Perkin–Elmer 580B spectrometer. The intensities of experimental IR bands were obtained by numerical integration.

Matrices were irradiated with the UV light from the high-pressure mercury lamp HBO 200 fitted with a water filter and a cut-off filter (WG 295) transmitting the light with $\lambda > 295$ nm. The time of the irradiation was 1 h.

3. Computational details

The geometries of planar C_{2h} and C_{2v} isomers of PBQDO were optimized at the *ab initio* MP2 level [13] using the standard 6-31++G(d,p) basis set. At the optimized geometries the relative electronic energies of the C_{2h} and C_{2v} isomers of PBQDO were calculated at the same level of theory. The MP2/6-31++G(d,p) method was also used to determine the barrier separating the PES minima corresponding to the C_{2h} and C_{2v} isomers in their ground electronic states.

For the $S_0 \rightarrow S_i$ (i = 1,2,3,4) transitions to the low-energy excited singlet states, the vertical excitation energies were calculated using the CC2 [14] as well as TD DFT(B3LYP) [15,16] methods. These calculations were carried out with the Turbomole program suite [17].

Potential energy surfaces of the S_1 and S_0 states of PBQDO were probed using the CASSCF method [18,19]. The active space employed in the CASSCF calculations consisted of 12 electrons correlated over eight molecular orbitals (six valence orbitals and two virtual orbitals). The computations at the CASSCF level were performed with the MOLPRO software package [20]. Dunning's correlation-consistent basis set [21] of double-ζ quality with polarization functions on all atoms (cc-pVDZ) was utilized in the CASSCF, CC2 and TD DFT calculations.

For C_{2h} and C_{2v} isomers of PBQDO, the ground electronic state harmonic vibrational frequencies and the absolute IR intensities were calculated using the density functional theory with the Becke's three-parameter exchange functional [22] and the gradient-corrected functional of Lee, Yang and Parr (DFT(B3LYP)) [23]. These calculations were carried out at geometries of the C_{2h} and C_{2v} forms optimized at the same DFT(B3LYP)/6-31++G(d,p) level. In order to perform the standard analysis of the calculated normal modes [24], the force constant matrices expressed in terms of Cartesian coordinates were transformed to the force constant matrices expressed in terms of molecule-fixed symmetry coordinates. The potential energy distribution (PED) matrices were calculated according to the standard procedures described in Refs. [25,26]. The symmetry coordinates used in this analysis (listed in Tables 2 and 3) were defined in the manner recommended by Pulay et al. [27]. The calculated PED matrix elements greater than 10% are given in Tables 4 and 5 (for C_{2h} and C_{2v} isomers, respectively). To approximately correct for the vibrational anharmonicity, the basis set truncation and the neglected part of the electron correlation, the calculated DFT wavenumbers were scaled down by a single factor of 0.98. The DFT and MP2 calculations were performed with the GAUSSIAN 03 program [28].

Table 1
CC2/cc-pVDZ and TD DFT/cc-pVDZ energy of vertical absorption (ΔE), dipole moment (μ), and oscillator strength (f) calculated at the ground-state equilibrium of the two isomeric forms of *para*-benzoquinone dioxime.

State	ΔE (eV)		μ (D)		f	
	CC2	TD DFT	CC2	TD DFT	CC2	TD DFT
C_{2h}-form						
S_0	0.0	0.0	0.0	0.0		
B_u ($^1\pi\pi^*$)	4.158	3.918	0.0		0.8724	0.6473
B_g ($^1n\pi^*$)	4.714	4.282	0.0		0.0	0.0
A_u ($^1n\pi^*$)	4.772	4.385	0.0		0.0030	0.0024
A_g ($^1\pi\pi^*$)	4.790	4.273	0.0		0.0	0.0
C_{2v}-form						
S_0	0.0	0.0	0.7100	0.5119		
B_2 ($^1\pi\pi^*$)	3.957	3.684	0.8042		0.6105	0.4074
B_1 ($^1n\pi^*$)	4.572	4.164	0.2556		0.0029	0.0023
A_2 ($^1n\pi^*$)	4.818	4.430	0.1741		0.0	0.0
B_2 ($^1\pi\pi^*$)	4.989	4.409	1.6412		0.1880	0.1373

At the CC2/cc-pVDZ level, the energy difference between the ground electronic states (S_0) of the C_{2h} and C_{2v} forms is equal $\Delta E = E(C_{2h}) - E(C_{2v}) = -2.146$ kJ mol^{-1} (−0.02224 eV).

4. Results and discussion

4.1. Relative energies of the C_{2h} and C_{2v} forms and the barrier separating the two minima

Relative energies of the C_{2h} and C_{2v} isomers of PBQDO were calculated using the MP2/6-31++G(d,p) method at geometries optimized at the same level. These calculations predicted the C_{2h} and C_{2v} forms to be nearly isoenergetic, with the C_{2h} form being slightly (by 1.8 kJ mol^{-1}) more stable. A similar result was obtained in analogous calculations carried out at the CASSCF/cc-pVDZ level of theory. The energy difference computed using the CASSCF method is 0.8 kJ mol^{-1}, in favor of the higher stability of the C_{2h} isomer. This result could be intuitively expected, because the interaction between the spatially well-separated oxime groups, which have different orientations in the two isomers, must be weak. Hence, the influence of the mutual orientation of the oxime groups on the total energy of the system should be very small.

The height of the barrier for the conversion of the C_{2h} isomer into the C_{2v} form (or *vice versa*) in the ground electronic state was assessed at the MP2/6-31++G(d,p) level. For the construction of the $C_{2h} \leftrightarrow C_{2v}$ isomerization path, the coordinate-driven minimum-energy-path approach was adopted. In these calculations one of the O—N=C—C torsional angles was chosen as the driving coordinate. For a series of fixed values of this torsional angle, all the remaining parameters defining the geometry of the system were optimized at the MP2/6-31++G(d,p) level. At each of these partially optimized geometries the MP2/6-31++G(d,p) energy was calculated (see Fig. 1). These calculations resulted in prediction of the energy of the transition point being higher by 218 kJ mol^{-1} than the energy of the C_{2h} planar isomer.

Table 2
Internal coordinates used in the normal mode analysis for the C_{2h} isomer of *para*-benzoquinone dioxime (atom numbering as in Scheme 1).

B_u	
$S_1 = r_{1,2} - r_{4,5}$	ν^1CC
$S_2 = r_{3,4} - r_{6,1}$	ν^2CC
$S_3 = r_{2,3} - r_{5,6}$	ν^3CC
$S_4 = r_{3,10} - r_{6,11}$	ν^1CH
$S_5 = r_{2,9} - r_{5,12}$	ν^2CH
$S_6 = r_{1,7} - r_{4,8}$	νCN
$S_7 = r_{7,13} - r_{8,14}$	νNO
$S_8 = r_{13,15} - r_{14,16}$	νOH
$S_9 = (6^{-1/2})(\beta_{6,2,1} - \beta_{1,3,2} + \beta_{2,4,3} - \beta_{3,5,4} + \beta_{4,6,5} - \beta_{5,1,6})$	βR1
$S_{10} = 1/2(\beta_{10,2,3} - \beta_{10,4,3} - \beta_{11,5,6} + \beta_{11,1,6})$	β^1CH
$S_{11} = 1/2(\beta_{12,4,5} - \beta_{12,6,5} - \beta_{9,1,2} + \beta_{9,3,2})$	β^2CH
$S_{12} = 1/2(\beta_{7,6,1} - \beta_{7,2,1} - \beta_{8,3,4} + \beta_{8,5,4})$	βCN
$S_{13} = (2^{-1/2})(\beta_{13,1,7} - \beta_{14,4,8})$	βNO
$S_{14} = (2^{-1/2})(\beta_{15,7,13} - \beta_{16,8,14})$	βOH
A_u	
$S_{15} = (12^{-1/2})(2\tau_{1,2,3,4} - \tau_{2,3,4,5} - \tau_{3,4,5,6} + 2\tau_{4,5,6,1} - \tau_{5,6,1,2,} - \tau_{6,1,2,3})$	τR1
$S_{16} = 1/2(\tau_{2,3,4,5} - \tau_{3,4,5,6} + \tau_{5,6,1,2} - \tau_{6,1,2,3})$	τR2
$S_{17} = 1/2(\tau_{13,7,1,6} + \tau_{13,7,1,2} + \tau_{14,8,4,3} + \tau_{14,8,4,5})$	τNO
$S_{18} = (2^{-1/2})(\tau_{15,13,7,1} + \tau_{16,14,8,4})$	τOH
$S_{19} = (2^{-1/2})(\gamma_{10,2,3,4} + \gamma_{11,5,6,1})$	γ^1CH
$S_{20} = (2^{-1/2})(\gamma_{9,1,2,3} + \gamma_{12,4,5,6})$	γ^2CH
$S_{21} = (2^{-1/2})(\gamma_{7,6,1,2} + \gamma_{8,3,4,5})$	γCN
A_g	
$S_{22} = r_{1,2} + r_{4,5}$	ν^4CC
$S_{23} = r_{3,4} + r_{6,1}$	ν^5CC
$S_{24} = r_{2,3} + r_{5,6}$	ν^6CC
$S_{25} = r_{3,10} + r_{6,11}$	ν^3CH
$S_{26} = r_{2,9} + r_{5,12}$	ν^4CH
$S_{27} = r_{1,7} + r_{4,8}$	ν^sCN
$S_{28} = r_{7,13} + r_{8,14}$	ν^sNO
$S_{29} = r_{13,15} + r_{14,16}$	ν^sOH
$S_{30} = 1/2(\beta_{1,3,2} - \beta_{2,4,3} + \beta_{4,6,5} - \beta_{5,1,6})$	βR2
$S_{31} = (12^{-1/2})(2\beta_{2,6,1} - \beta_{1,3,2} - \beta_{2,4,3} + 2\beta_{3,5,4} - \beta_{4,6,5} - \beta_{5,1,6})$	βR3
$S_{32} = 1/2(\beta_{10,2,3} - \beta_{10,4,3} + \beta_{11,5,6} - \beta_{11,1,6})$	β^3CH
$S_{33} = 1/2(\beta_{12,4,5} - \beta_{12,6,5} + \beta_{9,1,2} - \beta_{9,3,2})$	β^4CH
$S_{34} = 1/2(\beta_{7,6,1} - \beta_{7,2,1} + \beta_{8,3,4} - \beta_{8,5,4})$	β^sCN
$S_{35} = (2^{-1/2})(\beta_{13,1,7} + \beta_{14,4,8})$	β^sNO
$S_{36} = (2^{-1/2})(\beta_{15,7,13} + \beta_{16,8,14})$	β^sOH
B_g	
$S_{37} = (6^{-1/2})(\tau_{1,2,3,4} - \tau_{2,3,4,5} + \tau_{3,4,5,6} - \tau_{4,5,6,1} + \tau_{5,6,1,2,} - \tau_{6,1,2,3})$	τR3
$S_{38} = 1/2(\tau_{13,7,1,6} + \tau_{13,7,1,2} - \tau_{14,8,4,3} - \tau_{14,8,4,5})$	τ^sNO
$S_{39} = (2^{-1/2})(\tau_{15,13,7,1} - \tau_{16,14,8,4})$	τ^sOH
$S_{40} = (2^{-1/2})(\gamma_{10,2,3,4} - \gamma_{11,5,6,1})$	γ^3CH
$S_{41} = (2^{-1/2})(\gamma_{9,1,2,3} - \gamma_{12,4,5,6})$	γ^4CH
$S_{42} = (2^{-1/2})(\gamma_{7,6,1,2} - \gamma_{8,3,4,5})$	γ^sCN

$r_{i,j}$ is the distance between atoms A_i and A_j; $\beta_{i,j,k}$ is the angle between vectors A_kA_i and A_kA_j; $\tau_{i,j,k,l}$ is the dihedral angle between the plane defined by A_i, A_j, A_k and the plane defined by A_j, A_k, A_l atoms; $\gamma_{i,j,k,l}$ is the angle between the vector A_kA_i and the plane defined by atoms A_j, A_k, A_l.

Table 3
Internal coordinates used in the normal mode analysis for the C_{2v} isomer of *para*-benzoquinone dioxime (atom numbering as in Scheme 1).

A_1	
$S_1 = r_{1,2} + r_{3,4}$	ν^1CC
$S_2 = r_{4,5} + r_{6,1}$	ν^2CC
$S_3 = r_{2,3}$	νC2C3
$S_4 = r_{5,6}$	νC5C6
$S_5 = r_{2,9} + r_{3,10}$	ν^1CH
$S_6 = r_{5,12} + r_{6,11}$	ν^2CH
$S_7 = r_{1,7} + r_{4,8}$	ν^sCN
$S_8 = r_{7,13} + r_{8,14}$	ν^sNO
$S_9 = r_{13,15} + r_{14,16}$	ν^sOH
$S_{10} = (12^{-1/2})(2\beta_{2,6,1} - \beta_{1,3,2} - \beta_{2,4,3} + 2\beta_{3,5,4} - \beta_{4,6,5} - \beta_{5,1,6})$	βR1
$S_{11} = 1/2(\beta_{10,2,3} - \beta_{10,4,3} - \beta_{9,1,2} + \beta_{9,3,2})$	β^1CH
$S_{12} = 1/2(\beta_{12,4,5} - \beta_{12,6,5} - \beta_{11,5,6} + \beta_{11,1,6})$	β^2CH
$S_{13} = 1/2(\beta_{7,6,1} - \beta_{7,2,1} - \beta_{8,3,4} + \beta_{8,5,4})$	β^sCN
$S_{14} = (2^{-1/2})(\beta_{13,1,7} + \beta_{14,4,8})$	β^sNO
$S_{15} = (2^{-1/2})(\beta_{15,7,13} + \beta_{16,8,14})$	β^sOH
B_2	
$S_{16} = r_{1,2} - r_{3,4}$	ν^3CC
$S_{17} = r_{4,5} - r_{6,1}$	ν^4CC
$S_{18} = r_{2,9} - r_{3,10}$	ν^3CH
$S_{19} = r_{5,12} - r_{6,11}$	ν^4CH
$S_{20} = r_{1,7} - r_{4,8}$	ν^aCN
$S_{21} = r_{7,13} - r_{8,14}$	ν^aNO
$S_{22} = r_{13,15} - r_{14,16}$	ν^aOH
$S_{23} = 1/2(\beta_{1,3,2} - \beta_{2,4,3} + \beta_{4,6,5} - \beta_{5,1,6})$	βR2
$S_{24} = (6^{-1/2})(\beta_{2,6,1} - \beta_{1,3,2} + \beta_{2,4,3} - \beta_{3,5,4} + \beta_{4,6,5} - \beta_{5,1,6})$	βR3
$S_{25} = 1/2(\beta_{10,2,3} - \beta_{10,4,3} + \beta_{9,1,2} - \beta_{9,3,2})$	β^3CH
$S_{26} = 1/2(\beta_{12,4,5} - \beta_{12,6,5} + \beta_{11,5,6} - \beta_{11,1,6})$	β^4CH
$S_{27} = 1/2(\beta_{7,6,1} - \beta_{7,2,1} + \beta_{8,3,4} - \beta_{8,5,4})$	β^aCN
$S_{28} = (2^{-1/2})(\beta_{13,1,7} - \beta_{14,4,8})$	β^aNO
$S_{29} = (2^{-1/2})(\beta_{15,7,13} - \beta_{16,8,14})$	β^aOH
B_1	
$S_{30} = 1/2(\tau_{1,2,3,4} - \tau_{3,4,5,6} + \tau_{4,5,6,1} - \tau_{6,1,2,3})$	τR1
$S_{31} = 1/2(\tau_{13,7,1,6} + \tau_{13,7,1,2} - \tau_{14,8,4,3} - \tau_{14,8,4,5})$	τNO
$S_{32} = (2^{-1/2})(\tau_{15,13,7,1} - \tau_{16,14,8,4})$	τOH
$S_{33} = (2^{-1/2})(\gamma_{10,2,3,4} + \gamma_{9,1,2,3})$	γ^1CH
$S_{34} = (2^{-1/2})(\gamma_{11,5,6,1} + \gamma_{12,4,5,6})$	γ^2CH
$S_{35} = (2^{-1/2})(\gamma_{7,6,1,2} + \gamma_{8,3,4,5})$	γCN
A_2	
$S_{36} = (6^{-1/2})(\tau_{1,2,3,4} - \tau_{2,3,4,5} + \tau_{3,4,5,6} - \tau_{4,5,6,1} + \tau_{5,6,1,2,} - \tau_{6,1,2,3})$	τR2
$S_{37} = (12^{-1/2})(2\tau_{1,2,3,4} - \tau_{2,3,4,5} - \tau_{3,4,5,6} + 2\tau_{4,5,6,1} - \tau_{5,6,1,2,} - \tau_{6,1,2,3})$	τR3
$S_{38} = 1/2(\tau_{13,7,1,6} + \tau_{13,7,1,2} + \tau_{14,8,4,3} + \tau_{14,8,4,5})$	τ^aNO
$S_{39} = (2^{-1/2})(\tau_{15,13,7,1} + \tau_{16,14,8,4})$	τ^aOH
$S_{40} = (2^{-1/2})(\gamma_{10,2,3,4} - \gamma_{9,1,2,3})$	γ^3CH
$S_{41} = (2^{-1/2})(\gamma_{11,5,6,1} - \gamma_{12,4,5,6})$	γ^4CH
$S_{42} = (2^{-1/2})(\gamma_{7,6,1,2} - \gamma_{8,3,4,5})$	γ^aCN

$r_{i,j}$ is the distance between atoms A_i and A_j; $\beta_{i,j,k}$ is the angle between vectors A_kA_i and A_kA_j; $\tau_{i,j,k,l}$ is the dihedral angle between the plane defined by A_i, A_j, A_k and the plane defined by A_j, A_k, A_l atoms; $\gamma_{i,j,k,l}$ is the angle between the vector A_kA_i and the plane defined by atoms A_j, A_k, A_l.

However, it is clear that a MP2 assessment of the height of the barrier separating the C_{2h} and C_{2v} isomers should be treated with reservation. Close to the top of the barrier, intersection of two neighboring electronic states should be expected and such regions of the potential energy surface cannot be well described using single-reference methods (such as MP2). Hence, for description of the top of the barrier region, the multiconfigurational approach should be more adequate. The minimum-energy-path calculation of the top of the barrier separating the C_{2h} and C_{2v} forms of PBQDE, carried out at the CASSCF/cc-pVDZ level, resulted in prediction of the height of this barrier of 216 kJ mol^{-1}, with respect to the minimum corresponding to the C_{2h} isomer (Fig. 1).

Barriers of similar height are typical of a rotation around the double C=N bond in oximes (compare the calculations carried out for acetaldoxime [29] and N^4-hydroxycytosines [12]). Such a high barrier is likely to prevent flips around the double C=N bond even at elevated temperatures. However, it should be stressed that the calculations concern monomeric molecules, whereas the *syn–anti* conversion could be much easier for a compound in a condensed phase. The matrix-isolation study of acetaldoxime [29] demonstrated that the ratio of *syn* to *anti* isomers trapped in solid argon depends on the procedure and the conditions used during the preparation of the solid sample before it is used for the matrix deposition. Interestingly, for solid acetaldoxime, the *syn–anti* conversion was proven to occur even at temperatures lower than 273 K, despite the high-energy barrier (260 kJ mol^{-1}) predicted for isolated monomers of the compound.

4.2. Excited states of PBQDO and the conical intersection between S_0 and S_1

The energies of vertical transitions from the electronic ground S_0 state to the excited singlet states S_i (i = 1,2,3,4) were calculated using the CC2 and TD DFT methods, at geometries optimized (for the ground electronic state) at the MP2 and DFT levels, respectively. The results of these calculations are collected in Table 1, where the computed oscillator strengths of the $S_0 \rightarrow S_1$ electronic

Table 4
Experimental wavenumbers ($\tilde{\nu}$ cm^{-1}) and relative integrated intensities (I) of the bands in the spectrum of PBQDO isomer being the product of the photoreaction, compared with wavenumbers ($\tilde{\nu}$ cm^{-1}), absolute intensities (Ath, km mol^{-1}), and potential energy distribution (PED, %) theoretically calculated for the C_{2h} isomer of PBQDO.

Experimental – Ar matrix		Calculated – DFT(B3LYP)/6-31++G(d,p)			
$\tilde{\nu}$[a]	I	$\tilde{\nu}$[b]	Ath	Symm.[c]	PED[d]
3619	458	3743	436	B_u	νOH(100)
		3177	3	B_u	ν^1CH(95)
		3140	4	B_u	ν^2CH(95)
		1622	5	B_u	νCN(69)
		1593	8	B_u	ν^3CC(79)
1422	35	1422	26	B_u	β^1CH(35), βOH(25), ν^1CC(17), β^2CH(16)
1340/1331	106	1333	108	B_u	β^2CH(32), ν^2CC(19), ν^1CC(12), νCN(10)
1321	7				
1300/1297	200	1294	132	B_u	βOH(55), β^1CH(15), ν^1CC(10), ν^2CC(10)
1282	6				
1116	25	1117	20	B_u	β^2CH(34), β^1CH(33), ν^3CC(12)
		983	0.03	A_u	γ^2CH(66), γ^1CH(53)
972/961/956/947	641	973	776	B_u	νNO(81)
926	4	946	2	B_u	βR1(47), ν^1CC(21), ν^2CC(19)
870	17				
837/832	78	837	75	A_u	γ^1CH(46), γ^2CH(35), γCN(24)
783	15				
764	41	768	49	B_u	ν^2CC(34), βR1(25), βNO(13), νCN(12)
739	21				
		538	17	A_u	γCN(29), τOH(24), τNO(20), τR1(14)
530/525	72	525	43	B_u	βNO(52), ν^1CC(18), νNO(10)
431	9	433	7	A_u	τR1(73), τNO(12), γCN(11)
398	211	399	238	A_u	τOH(68), γCN(22)
		244	2	A_u	τNO(56), τR1(31), τR2(15)
		197	2	B_u	βCN(67), βNO(23)
		68	0.004	A_u	τR2(75), γCN(14), τNO(12)

[a] Wavenumbers of the strongest bands are underlined.
[b] Theoretical wavenumbers were scaled by a factor of 0.98.
[c] Symmetry.
[d] PED's lower than 10% are not included. Symmetry coordinates used in the normal mode analysis are given in Table 2.

transitions are also presented. For both C_{2h} and C_{2v} isomers, these data show that the lowest-energy excited singlet states (S_1) should have the $\pi\pi^*$ orbital nature. According to the CC2 and TD DFT calculations, for C_{2h} as well as for C_{2v} forms, the transitions from S_0 to S_1 are strongly allowed ($f > 0.4$). In comparison to the very strong $S_0 \rightarrow S_1$ absorptions, other $S_0 \rightarrow S_i$ ($i = 2, 3, 4$) electronic transitions should be significantly less intense. Some of those $S_0 \rightarrow S_i$ ($i = 2, 3, 4$) transitions are forbidden by symmetry, some others are allowed, but their oscillator strengths are much lower than those of the $S_0 \rightarrow S_1$ transitions (see Table 1). Hence, a broad-band UV irradiation of PBQDO molecule is expected to result mainly in promotion of the system to the S_1 state.

The search for a conical intersection (CI) between the ground electronic state and the lowest excited singlet state (S_1) was performed with the CASSCF method. The conformation with perpendicular orientation of one of the hydroxylimino group was chosen as the starting structure for the search of the lowest-energy CI seam between S_1 and S_0 states. The geometry of the CI point was fully optimized using the state-averaged CASSCF calculations. The optimized structure of the molecule at the conical intersection (CI) is presented in Fig. 2. In this structure one of the hydroxylimino groups is approximately perpendicular to the plane of the six-membered ring (at CI, the optimized value of the O13-N7=C1–C6 torsional angle is 90.8°), whereas the other hydroxylimino group remains virtually coplanar with the ring. Noteworthy is also the position of the hydrogen atom attached to O13. This H-atom is not coplanar with O13, N7 and C1, but it is twisted towards C6. The HOMO and LUMO natural orbitals, resulting from the CASSCF calculation at the optimized CI point, are also shown in Fig. 2.

In the multidimensional space of internal coordinates defining the geometry of PBQDO molecule, a linearly interpolated internal coordinate (Li–IC) reaction path was constructed. The internal coordinates at the Li–IC points change proportionally between coordinates describing the point of the conical intersection (CI) and one of the C_{2v} (or C_{2h}) minima. At the jth point of the Li–IC the value of the ith internal coordinate s_i is given by:

$$s_i^{(j)} = s_i^{(CI)} + (s_i^{(Min)} - s_i^{(CI)}) \cdot a^{(j)}, \quad i = 1, \ldots, 3N-6.$$

$s_i^{(CI)}$ is the value of the s_i internal coordinate at the CI geometry,
$s_i^{(Min)}$ is the value of the s_i internal coordinate at the geometry of the C_{2h} (or C_{2v}) minimum in S_0.
$a^{(j)}$ is a factor fixed for a jth point of the Li–IC at a value between 0 and 1.

Along the Li–IC paths, a series of single-point CASSCF calculations of S_0 and S_1 energies were carried out. In such a manner, potential energy profiles of S_0 and S_1 states were obtained. The results presented in Fig. 3 show that, after excitation to one of the Franck–Condon regions in S_1, the system should barrierlessly relax to the CI area.

Since out-of-plane rotation of one of the hydroxylimino groups leads to lowering of the energy of the S_1 state of PBQDO, it was interesting if rotation of both hydroxylimino (C=N—OH) groups would have the same (or perhaps even more pronounced) consequence. In order to test this possibility, a search for conical intersections between S_0 and S_1 was carried out, starting from the structures TS1 and TS2 presented in Fig. 4. However, optimizations for a CI point (performed at the CASSCF level) did not converge to structures similar to TS1 nor TS2. On the contrary, optimizations starting from TS1 or TS2 led to a conical intersection point with only one hydroxylimino group perpendicular to the ring. This optimized CI structure was identical to that presented in Fig. 2.

Because at the CI geometry one of the hydroxylimino groups is nearly perpendicular to the six-membered ring of PBQDO, it can be expected that radiationless decay from CI to the minima in S_0

Table 5
Experimental wavenumbers ($\tilde{\nu}$ cm^{-1}) and relative integrated intensities (I) of the bands in the spectrum of PBQDO isomer being the substrate of the photoreaction, compared with wavenumbers ($\tilde{\nu}$ cm^{-1}), absolute intensities (Ath, km mol^{-1}), and potential energy distribution (PED, %) theoretically calculated for the C_{2v} isomer of PBQDO.

Experimental – Ar matrix		Calculated – DFT(B3LYP)/6-31++G(d,p)			
$\tilde{\nu}$[a]	I	$\tilde{\nu}$[b]	Ath	Symm.[c]	PED[d]
		3745	12	A_1	ν^sOH(97)
3621	474	3744	424	B_2	ν^aOH(97)
		3177	1	A_1	ν^1CH(99)
		3162	1	B_2	ν^3CH(100)
		3156	5	A_1	ν^2CH(99)
		3140	0.0002	B_2	ν^4CH(100)
		1657	1	A_1	νC5C6(38), νC2C3(24), βR1(10)
		1620	3	B_2	ν^aCN(69)
		1594	1	A_1	νC2C3(44), νC5C6(34)
		1571	0.03	A_1	ν^sCN(68), β^sOH(15)
		1448	6	B_2	ν^4CC(37), β^4CH(28)
		1401	1	B_2	β^3CH(58), ν^3CC(16), β^aOH(15)
1355	26	1361	46	A_1	β^sOH(34), ν^2CC(20), ν^sCN(10)
1316/<u>1309</u>	123	1314	111	B_2	β^aOH(49), β^4CH(31), ν^aCN(11)
<u>1301</u>/1295	94	1297	70	A_1	β^sOH(46), ν^1CC(17), ν^2CC(13), β^2CH(11)
1272	5	1266	6	B_2	β^3CH(29), β^4CH(26), β^aOH(16), ν^3CC(10)
1154	7	1166	8	A_1	β^1CH(54), β^2CH(26)
1117	11	1116	9	A_1	β^2CH(48), β^1CH(20)
1002	38	986	68	A_1	ν^sNO(85)
979/<u>969</u>	610	977	688	B_2	ν^aNO(81)
912	25				
		945	0.2	B_2	βR3(49), ν^4CC(20), ν^3CC(19)
864	12				
840	87	839	71	B_1	γ^1CH(51), γ^2CH(29), γCN(24)
801	15				
		794	0.4	A_1	ν^1CC(53), ν^2CC(22)
776	46	779	32	B_2	ν^3CC(32), βR3(23), β^aNO(15), ν^aCN(11)
769	13	776	3	B_1	V^2CH(64), γ^1CH(33)
601	20	598	13	B_2	βR2(69), ν^4CC(12)
591	22	596	23	A_1	β^sNO(47), βR1(24), ν^2CC(15)
557	27	553	33	B_2	β^aNO(47), β^aCN(15), ν^aNO(12), ν^4CC(12)
504	18	514	32	B_1	γCN(36), τOH(34), γ^1CH(13)
394	188	398	223	B_1	τOH(61), γCN(28)
		373	1	A_1	βR1(58)
		291	10	B_1	τNO(79), τR1(14)
		287	4	B_2	β^aCN(55), β^aNO(35)
		189	0.1	A_1	β^sCN(63), β^sNO(26)
		72	0.02	B_1	τR1(79), γCN(11), τNO(10)

[a] Wavenumbers of the strongest bands are underlined.
[b] Theoretical wavenumbers were scaled by a factor of 0.98.
[c] Symmetry.
[d] PED's lower than 10% are not included. Symmetry coordinates used in the normal mode analysis are given in Table 3.

should yield either C_{2h} isomer or C_{2v} isomer, or a mixture of these two forms. The quasisymmetric shape of the plot in Fig. 3 (with respect to the torsion around N7=C1 bond) might suggest that the photoreaction, induced by UV irradiation of PBQDO, might lead to a photostationary state.

To the best of our knowledge, the experimental and theoretical investigations of syn–anti photoisomerizations in molecules with oxime group directly attached to a six-membered ring are restricted, so far, to the studies on N^4-hydroxycytosines [3,4,12]. In these works it was demonstrated that UV-induced syn–anti phototransformations in these compounds lead, in general, to a photostationary state. However, these photoreactions have not always yielded a photostationary mixture with each of the isomers populated enough to be easily detectable. In some cases (e.g. for 1,3-dimethyl-N^4-hydroxycytosine [12] or for N^2-hydroxyisocytosine [11]), the position of the photostationary state was shifted very much in favor of high population of a photoproduct (and an almost total conversion was observed), whereas for other derivatives (such as 1,5-dimethyl-N^4-hydroxycytosine [12]), the photostationary state was shifted strongly towards high population of the substrate (and no phototransformation was observed). The studies on N^4-hydroxycytosines led to the conclusion that, although the general theoretical picture of syn–anti photoisomerizations in compounds with oxime group directly attached to a planar ring is known, the quantitative (or semiquantitative) prediction of the position of the expected final photostationary state is still beyond the current capabilities of computational photochemistry.

4.3. Experimental studies of matrix-isolated monomers of PBQDO

Within the current work, several low-temperature argon matrices with isolated molecules of PBQDO were prepared, monitored using IR spectroscopy, irradiated with UV and monitored again by taking their IR spectra. In all the cases, matrices were prepared by codeposition of large excess of Ar and monomers of PBQDO sublimating from a solid heated to 360 K. The depositions differed from each other by the conditions under which the solid samples of PBQDO were prepared before the matrix experiment. A solid PBQDO sample, which had never been warmed to temperature higher than 383 K, was used in one type of matrix-isolation experiments, whereas in other experiments matrices were deposited form solid PBQDO that (prior to the matrix-isolation experiment) had been heated under vacuum to 433 K (in a sealed glass sublimation tube). It turned out that the IR spectra of PQBDO monomers, recorded in these two types of experiments, were not identical. Representative fragments of the IR spectra recorded in each of

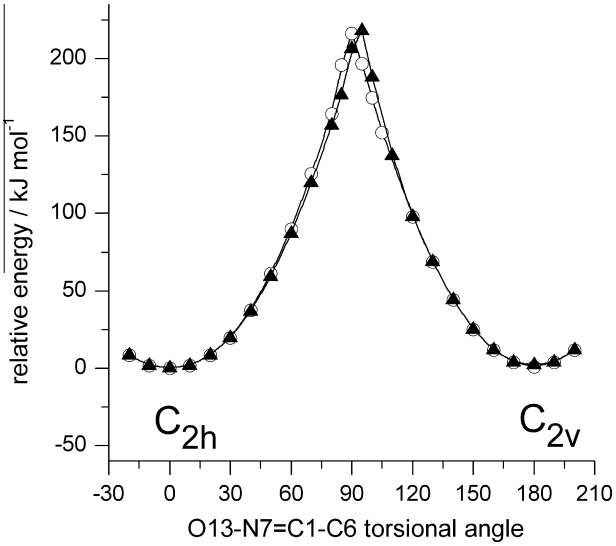

Fig. 1. Barrier for interconversion between the two isomers of PBQDO obtained by the calculations carried out at the MP2/6-31++G(d,p) level (triangles) or at the CASSCF/cc-pVDZ level (open circles). At each point a value of the O13-N7=C1-C6 torsional angle (see Scheme 1) was fixed, all remaining geometry parameters optimized and the energy was calculated. At each point the optimized value of the O14—N8=C4—C5 torsion was 180 ± 10°.

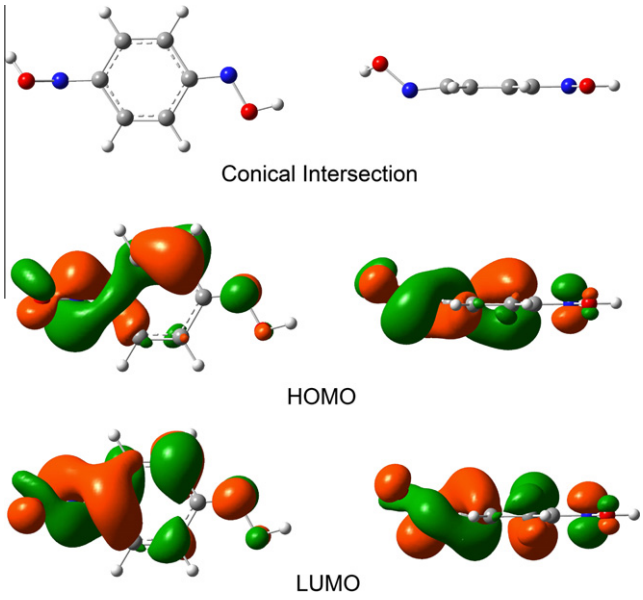

Fig. 2. The optimized (CASSCF) structure of PBQDO at the point of conical intersection (CI) between the S_0 and S_1 states. HOMO and LUMO natural orbitals calculated for the CI geometry using the CASSCF method. The structure as well as natural orbitals are presented as two projections with the six-membered ring perpendicular (right panel) or parallel (left panel) to the plane of observation.

the experiment types are compared in Fig. 5. It is easy to notice that in the spectrum presented in Fig. 5B there appears a second set of IR bands, with respect to the spectrum shown in Fig. 5A. The two sets of bands can be interpreted as the spectral indications of two (C_{2h} and C_{2v}) isomers of PBQDO, populated in different proportions in the two types of experiments. Whereas in the matrix corresponding to the spectrum A (in Fig. 5) one of the isomers strongly dominates, in the matrix corresponding to the spectrum B (in Fig. 5) both forms are significantly populated.

The UV ($\lambda > 295$ nm) irradiation of a matrix containing both isomers in nearly equal abundance (that is the matrix deposited from

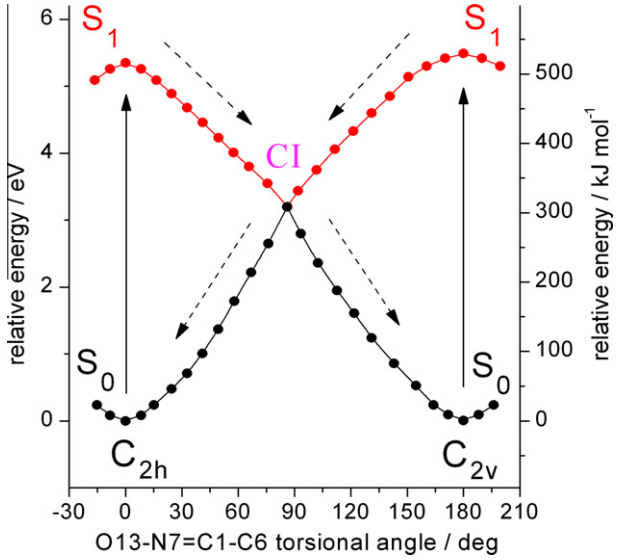

Fig. 3. Potential energy profiles calculated for the ground S_0 and the first excited singlet S_1 states of PBQDO using the CASSCF/cc-pVDZ methods. The points on PE surfaces of S_0 and S_1 were calculated along the linearly interpolated coordinate connecting the C_{2h} (or C_{2v}) minima with the point of conical intersection (CI).

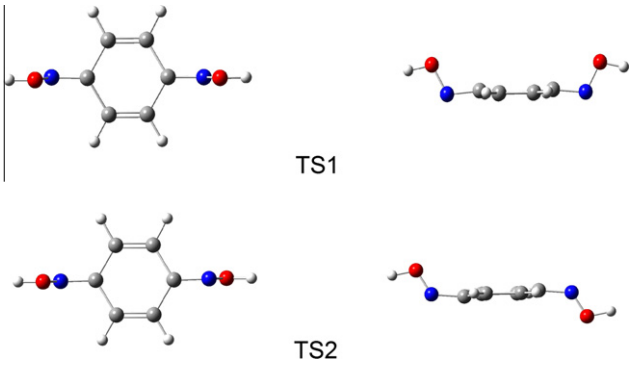

Fig. 4. Structures of PBQDO conformations with oxime groups perpendicular to the six-membered ring.

a solid sample heated before the experiment to 433 K) resulted in pronounced changes in the relative intensities of the bands in the IR spectrum. One set of bands, marked with asterisk in Fig. 6, disappeared almost completely upon the UV irradiation, whereas the intensities of the bands from the other set increased by nearly 100%. The spectrum recorded after the UV irradiation was virtually identical with that shown in Fig. 5A (see also the comparison presented in Fig. 7). These experimental findings strongly suggest that upon UV irradiation one of the isomers of PBQDO converts into the other and the observed photoreaction concerns rotation of one of the hydroxylimino groups by 180°.

In order to determine which of the isomers of PBQDO is the substrate and which is the product of the photoreaction, the experimental IR spectra of both isomers of PBQDO were separated via electronic subtraction and compared with the spectra theoretically predicted at the DFT(B3LYP)/6-31++G(d,p) level for the C_{2v} and C_{2h} structures. This comparison is presented in Fig. 8. In spite of different symmetry, implying different number of the IR-active modes, the theoretical spectra of both PBQDO isomers are quite similar. The strongest bands predicted for the C_{2h} form have their counterparts at very similar frequencies in the spectrum of the C_{2v} isomer. As usual in the IR spectra of oximes the strongest bands are due to the stretching vibrations of the N-O bonds. In the calculated spec-

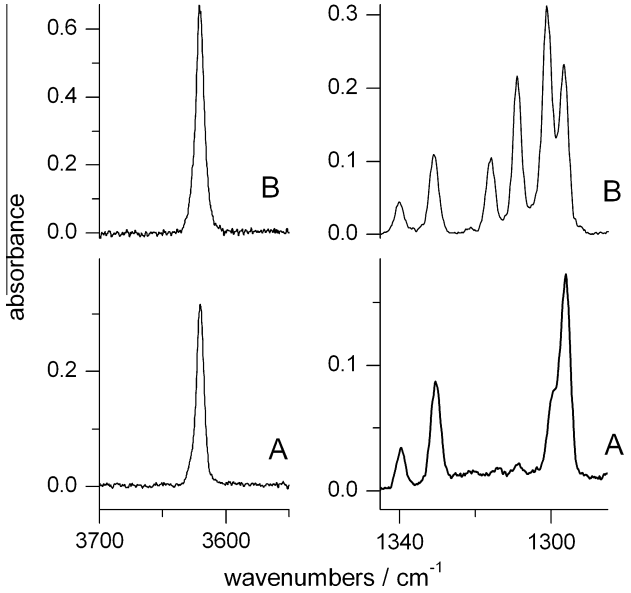

Fig. 5. Portions of infrared spectra of PBQDO isolated in Ar matrices. The monomers of PBQDO were deposited by sublimation (at 360 K) of two solid PBQDO samples: (A) the solid has never been warmed to temperature higher than 383 K; (B) prior to the matrix-isolation experiment the solid was heated (under vacuum, in a sealed glass sublimation tube) to 433 K.

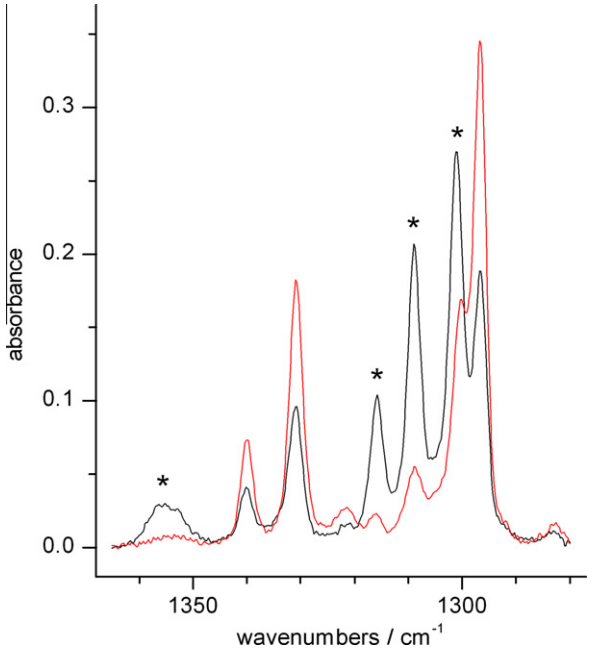

Fig. 6. Portion of the infrared spectrum of PBQDO isolated in an Ar matrix: (black line) spectrum of matrix-isolated monomers of PBQDO deposited by sublimation of a solid PBQDO sample heated (prior to the matrix-isolation experiment) to 433 K; (red line) spectrum of the same matrix recorded after 1 h of irradiation with UV light ($\lambda > 295$ nm). Asterisks indicate the bands due to the form consumed in the photoreaction. (For interpretation of the references to colour in this figure legend, the reader is referred to the web version of this article.)

tra of both PBQDO isomers these bands have frequencies differing only by 4 cm^{-1}. The strong bands observed at *ca.* 970 cm^{-1} in the spectra of both forms partially overlap. Also the strong bands due to the stretching and torsional vibrations of the OH groups (at 3620 cm^{-1} and at *ca.* 400 cm^{-1}, respectively) were observed for the two isomers at practically the same positions (see Figs. 5 and 8). Hence, the identification of the forms being the substrate and

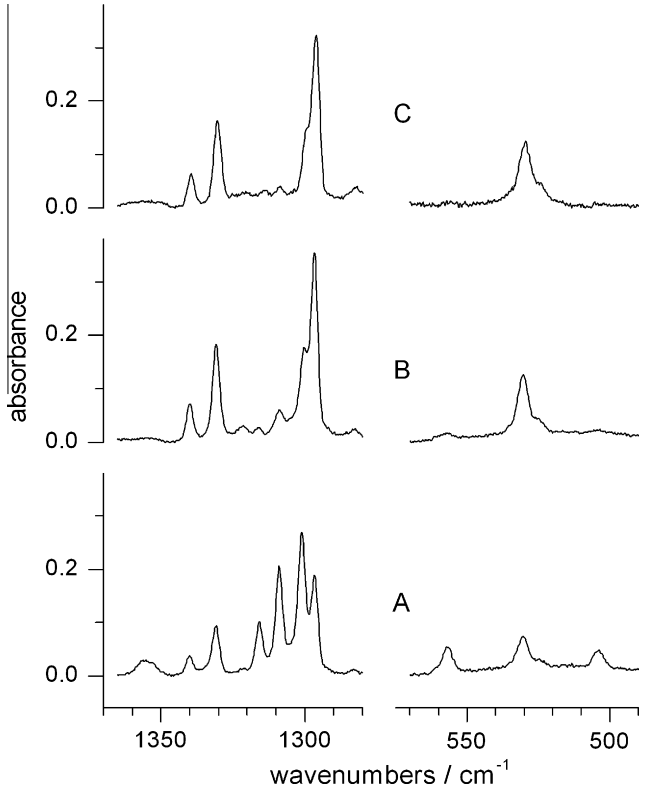

Fig. 7. Two portions of the infrared spectra of PBQDO isolated in Ar matrices: (A) matrix deposited from a solid PBQDO sample heated (prior to the matrix-isolation experiment) to 433 K; (B) the same matrix after 1 h of UV ($\lambda > 295$ nm) irradiation; (C) matrix deposited from a solid PBQDO sample that has never been warmed to temperature higher than 383 K.

the product of the photoreaction had to rely on the analysis of lower-intensity bands. In this respect, the bands observed at frequencies near 1300 cm^{-1} and in the 600–500 cm^{-1} range were particularly useful. The comparison of the experimental and the theoretical spectral patterns in these regions (Fig. 8) allowed a reliable assignment of the photoproduced species to the C_{2h} isomer. Similarly, the substrate of the photoreaction could be readily assigned to the C_{2v} form.

The detailed assignment of the experimental IR bands observed in the spectra of the C_{2h} and C_{2v} forms of PBQDO to the theoretically calculated normal modes is presented in Tables 4 and 5.

5. Concluding discussion

Both C_{2v} and C_{2h} isomers of PBQDO were observed in matrix-isolation experiments carried out in the present work. The relative populations of the two isomers trapped in low-temperature matrices depended on the way the solid sample of the compound was prepared prior to a matrix-isolation experiment. In matrices deposited from a solid that was not subject to warming above 383 K only the more stable C_{2h} isomer was populated, whereas both C_{2h} and C_{2v} isomers were nearly equally populated in matrices deposited from a solid sample of PBQDO heated before the experiment to 433 K.

The very observation of different ratios of C_{2h} and C_{2v} isomers in matrices prepared using solid samples of PBQDO treated thermally in a different way, clearly demonstrates that during deposition of a matrix (that is during a process where the solid PBQDO is warmed only to moderate temperature 360 K) the isomers do not transform into each other. This is the result of a high-energy barrier separating these two forms. However, for a solid PBQDO at higher temper-

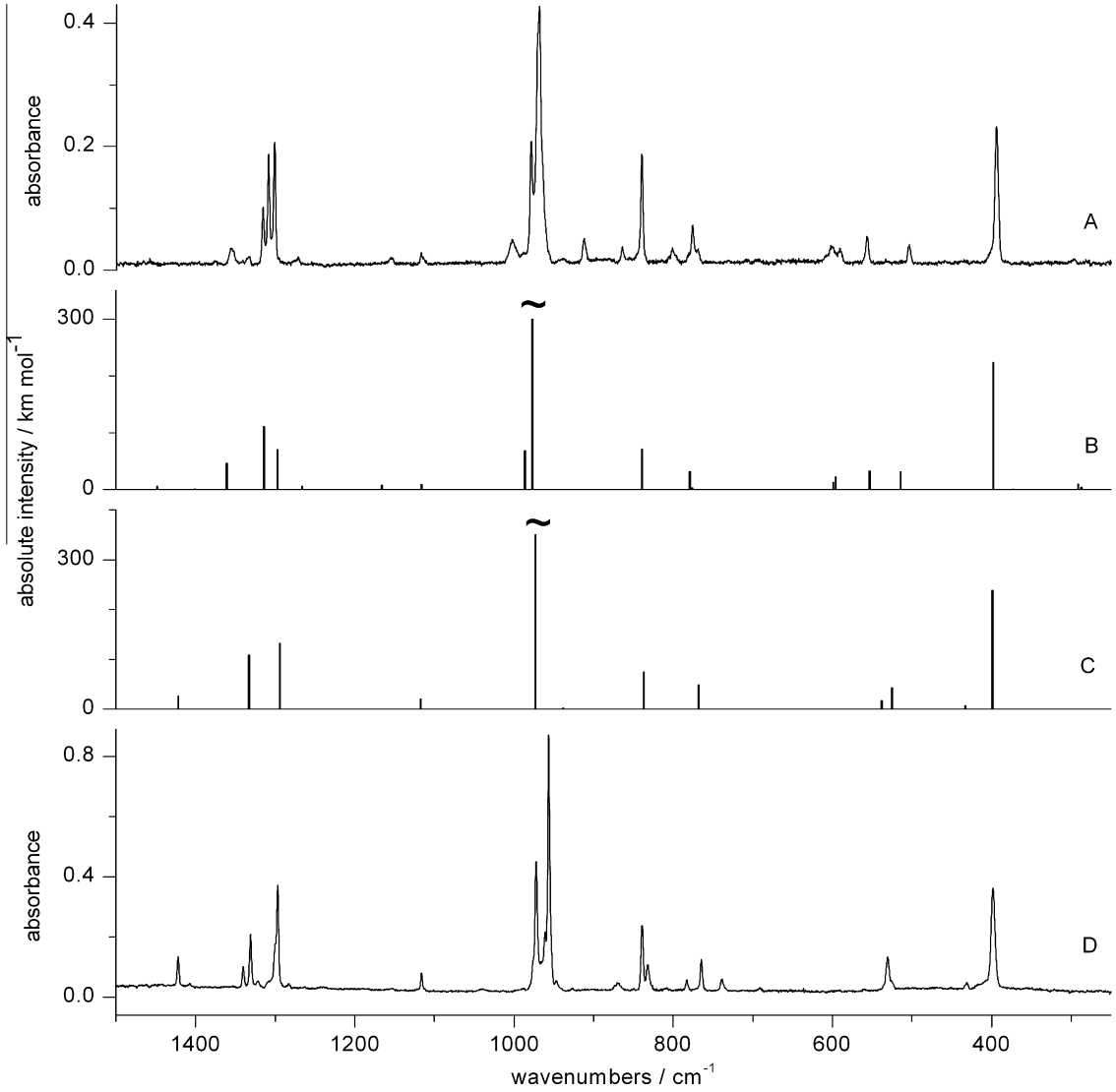

Fig. 8. (A) experimental spectrum of the PBQDO isomer being a substrate of the photoreaction; (B) theoretically predicted infrared spectrum of the C_{2v} isomer of PBQDO; (C) theoretical spectrum of the C_{2h} isomer; (D) experimental spectrum of the isomer being a photoproduct. Baseline of the experimental spectra was corrected. Theoretical frequencies obtained at the DFT(B3LYP)/6-31++G(d,p) level were scaled by 0.98. The most intense theoretical bands at 977 cm^{-1} (trace B) and 973 cm^{-1} (trace C) are not presented in full height. The intensities are 688 and 776 km mol^{-1}, respectively.

ature 433 K, the change of isomeric form is possible and thermodynamic equilibrium between the C_{2h} and C_{2v} forms (or a state close to the equilibrium) is achieved. For matrices deposited from such solid samples of PBQDO, the $[C_{2h}]$:$[C_{2v}]$ ratio of isomers approximately equal to 1:1 was revealed by comparison of the spectra recorded before and after the UV-induced photoreaction converting the C_{2v} isomer into the C_{2h} form. Increase by 100% of the bands assigned to form C_{2h}, accompanied by almost total disappearance of the spectrum of isomer C_{2v}, demonstrated that before UV irradiation a nearly equimolar mixture of the isomers was isolated in the matrix. Such an equimolar mixture should approximately correspond to thermal equilibrium of two isomers, which, according to theoretical predictions, should be very close in energy.

A very effective photochemical interconversion between the C_{2v} and C_{2h} isomers of PBQDO was theoretically predicted by identification of the conical intersection (CI) seam between S_1 and S_0 electronic states. At the CI point the PBQDO molecule adopts an intermediate structure between the two stable C_{2v} and C_{2h} forms, with one of the hydroxylimino groups perpendicular to the plane of the six-memebered ring. Experimental observations of the photoisomerization in PBQDO clearly show that the final stage of this (in principle photoreversible) reaction is shifted very strongly towards nearly exclusive population of the C_{2h} form.

References

[1] N.J. Turro, Modern Molecular Photochemistry, University Science Books, Sausalito, California, 1991 (Chapter 12).
[2] M. Klessinger, J. Michl, Excited States and Photochemistry of Organic Molecules, VCH Publishers, New York, 1995 (Chapter 7.1).
[3] T. Stepanenko, L. Lapinski, A. Sobolewski, M.J. Nowak, B. Kierdaszuk, J. Phys. Chem. A 104 (2000) 9459.
[4] L. Lapinski, M.J. Nowak, L. Adamowicz, Photochem. Photobiol. 74 (2001) 253.
[5] G. Ciamician, P. Silber, Berichte 36 (1904) 4266.
[6] O.L. Brady, F.P. Dunn, J. Chem. Soc. 103 (1913) 1619.
[7] A.C. Pratt, Chem. Soc. Rev. 6 (1977) 63.
[8] A. Padwa, Chem. Rev. 77 (1977) 37.
[9] P. Yates, J. Wong, S. McLean, Tetrahedron 37 (1981) 3357.
[10] H. Suginome, K. Ohshima, Y. Ohue, T. Ohki, H. Senboku, J. Chem. Soc. Perkin Trans. I (1994) 3239.
[11] L. Lapinski, M.J. Nowak, J.S. Kwiatkowski, J. Leszczynski, Photochem. Photobiol. 77 (2003) 243.
[12] L. Lapinski, M.J. Nowak, A.L. Sobolewski, B. Kierdaszuk, J. Phys. Chem. A 110 (2006) 5038.
[13] C. Møller, M.S. Plesset, Phys. Rev. 46 (1934) 618.
[14] O. Christiansen, H. Koch, P. Jørgensen, Chem. Phys. Lett. 243 (1995) 409.
[15] R. Bauernschmitt, R. Ahlrichts, J. Am. Chem. Soc. 120 (1998) 5052.

[16] R. Bauernschmitt, R. Ahlrichts, Chem. Phys. Lett. 256 (1996) 454.
[17] TURBOMOLE V5-8-0, A development of University of Karlsruhe and Forschungszentrum Karlsruhe GmbH, <http://www.turbomole.com>, 2005.
[18] B.O. Roos, P.R. Taylor, P.E.M. Siegbahn, Chem. Phys. 48 (1980) 157.
[19] B.O. Roos, Adv. Chem. Phys. 69 (1987) 399.
[20] MOLPRO, Version 2008.1, A package of ab initio programs, H.-J. Werner, P.J. Knowles, R. Lindh, F.R. Manby, M. Schütz, P. Celani, T. Korona, A. Mitrushenkov, G. Rauhut, T.B. Adler, R.D. Amos, A. Bernhardsson, A. Berning, D.L. Cooper, M.J.O. Deegan, A.J. Dobbyn, F. Eckert, E. Goll, C. Hampel, G. Hetzer, T. Hrenar, G. Knizia, C. Köppl, Y. Liu, A.W. Lloyd, R.A. Mata, A.J. May, S.J. McNicholas, W. Meyer, M.E. Mura, A. Nicklass, P. Palmieri, K. Pflüger, R. Pitzer, M. Reiher, U. Schumann, H. Stoll, A.J. Stone, R. Tarroni, T. Thorsteinsson, M. Wang, A. Wolf, <http://www.molpro.net>.
[21] D.E. Woon, T.H. Dunning Jr., J. Chem. Phys. 98 (1993) 1358.
[22] A.D. Becke, Phys. Rev. A 38 (1988) 3098.
[23] C.T. Lee, W.T. Yang, R.G. Parr, Phys. Rev. B 37 (1988) 785.
[24] J.H. Schachtschneider, Technical Report, Shell Development Co., Emeryville, CA, 1969.
[25] G. Keresztury, G. Jalsovszky, J. Mol. Struct. 10 (1971) 304.
[26] H. Rostkowska, L. Lapinski, M.J. Nowak, Vib. Spectrosc. 49 (2009) 43.
[27] P. Pulay, G. Fogarasi, F. Pang, J.E. Boggs, J. Am. Chem. Soc. 101 (1979) 2550.
[28] M.J. Frisch, G.W. Trucks, H.B. Schlegel, G.E. Scuseria, M.A. Robb, J.R. Cheeseman, J.A. Montgomery, Jr., T. Vreven, K.N. Kudin, J.C. Burant, J.M. Millam, S.S. Iyengar, J. Tomasi, V. Barone, B. Mennucci, M. Cossi, G. Scalmani, N. Rega, G.A. Petersson, H. Nakatsuji, M. Hada, M. Ehara, K. Toyota, R. Fukuda, J. Hasegawa, M. Ishida, T. Nakajima, Y. Honda, O. Kitao, H. Nakai, M. Klene, X. Li, J.E. Knox, H.P. Hratchian, J.B. Cross, C. Adamo, J. Jaramillo, R. Gomperts, R.E. Stratmann, O. Yazyev, A.J. Austin, R. Cammi, C. Pomelli, J.W. Ochterski, P.Y. Ayala, K. Morokuma, G.A. Voth, P. Salvador, J.J. Dannenberg, V.G. Zakrzewski, S. Dapprich, A.D. Daniels, M.C. Strain, O. Farkas, D.K. Malick, A.D. Rabuck, K. Raghavachari, J.B. Foresman, J.V. Ortiz, Q. Cui, A.G. Baboul, S. Clifford, J. Cioslowski, B.B. Stefanov, G. Liu, A. Liashenko, P. Piskorz, I. Komaromi, R.L. Martin, D.J. Fox, T. Keith, M.A. Al-Laham, C.Y. Peng, A. Nanayakkara, M. Challacombe, P.M.W. Gill, B. Johnson, W. Chen, M.W. Wong, C. Gonzalez, J.A. Pople, Gaussian 03, Revision A.1, Gaussian, Inc., Pittsburgh PA, 2003.
[29] A. Andrzejewska, L. Lapinski, I. Reva, R. Fausto, Phys. Chem. Chem. Phys. 4 (2002) 3289.